

Research and application of composite stochastic resonance in enhancement detection

Rui Gao(高蕊), Shangbin Jiao(焦尚彬), and Qiongjie Xue(薛琼婕)
Citation: Chin. Phys. B, 2024, 33 (**1**): 010203. DOI: 10.1088/1674-1056/ad01a8
Journal homepage: http://cpb.iphy.ac.cn; http://iopscience.iop.org/cpb

What follows is a list of articles you may be interested in

Intervention against information diffusion in static and temporal coupling networks

Yun Chai(柴允), You-Guo Wang(王友国), Jun Yan(颜俊), and Xian-Li Sun(孙先莉)
Chin. Phys. B, 2023, 32 (**9**): 090202. DOI: 10.1088/1674-1056/acb9f4

Angle robust transmitted plasmonic colors with different surroundings utilizing localized surface plasmon resonance

Xufeng Gao(高旭峰), Qi Wang(王琦), Shijie Zhang(张世杰), Ruijin Hong(洪瑞金), and Dawei Zhang(张大伟)
Chin. Phys. B, 2023, 32 (**7**): 070204. DOI: 10.1088/1674-1056/ac921e

Weak signal detection method based on novel composite multistable stochastic resonance

Shangbin Jiao(焦尚彬), Rui Gao(高蕊), Qiongjie Xue(薛琼婕), and Jiaqiang Shi(史佳强)
Chin. Phys. B, 2023, 32 (**5**): 050202. DOI: 10.1088/1674-1056/aca4bd

Meshfree-based physics-informed neural networks for the unsteady Oseen equations

Keyi Peng(彭珂依), Jing Yue(岳靖), Wen Zhang(张文), and Jian Li(李剑)
Chin. Phys. B, 2023, 32 (**4**): 040207. DOI: 10.1088/1674-1056/ac9cb9

Local density of optical states calculated by the mode spectrum in stratified media

Ting Fu(傅廷), Jingxuan Chen(陈静瑄), Xueyou Wang(王学友), Yingqiu Dai(戴迎秋), Xuyan Zhou(周旭彦), Yufei Wang(王宇飞), Mingjin Wang(王明金), and Wanhua Zheng(郑婉华)
Chin. Phys. B, 2023, 32 (**4**): 040204. DOI: 10.1088/1674-1056/acaf2c

---

Research and application of composite stochastic resonance in enhancement detection

Rui Gao(高蕊)[1,2], Shangbin Jiao(焦尚彬)[1,3,†], and Qiongjie Xue(薛琼婕)[1,3]

[1] *School of Automation and Information Engineering, Xi'an University of Technology, Xi'an* 710048, *China*
[2] *School of Electronic and Electrical Engineering, Baoji University of Arts and Sciences, Baoji* 721016, *China*
[3] *Shaanxi Key Laboratory of Complex System Control and Intelligent Information Processing, Xi'an University of Technology, Xi'an* 710048, *China*

(Received 16 September 2023; revised manuscript received 8 October 2023; accepted manuscript online 10 October 2023)

Aiming at the problem that the intermediate potential part of the traditional bistable stochastic resonance model cannot be adjusted independently, a new composite stochastic resonance (NCSR) model is proposed by combining the Woods–Saxon (WS) model and the improved piecewise bistable model. The model retains the characteristics of the independent parameters of WS model and the improved piecewise model has no output saturation, all the parameters in the new model have no coupling characteristics. Under α stable noise environment, the new model is used to detect periodic signal and aperiodic signal, the detection results indicate that the new model has higher noise utilization and better detection effect. Finally, the new model is applied to image denoising, the results showed that under the same conditions, the output peak signal-to-noise ratio (PSNR) and the correlation number of NCSR method is higher than that of other commonly used linear denoising methods and improved piecewise SR methods, the effectiveness of the new model is verified.

Keywords: Woods–Saxon, improved piecewise model, composite stochastic resonance (SR), image denoising

PACS: 02.60.Cb, 05.40.–a, 05.40.Fb, 05.45.–a **DOI:** 10.1088/1674-1056/ad01a8

1. Introduction

The main difference between the stochastic resonance (SR) weak signal detection method and the traditional method is the use of the beneficial nature of noise. The SR theory was proposed by Benzi *et al.* when studying the cycle of the glacial period,[1] it has become a hot research topic in the field of nonlinear science. With the continuous exploration and development of SR theory, it has been applied in many fields such as electronic systems,[2,3] quantum systems,[4] signal processing,[5,6] image enhancement,[7,8] mechanical systems,[9–12] neural networks,[13–15] chemistry and biology,[17–19] among which weak signal detection is the most widely used. The detection effect of SR method is greatly related to the nonlinear model in SR system. The commonly used SR models are monostable, bistable, and tristable, Qiao *et al.*[20] proved that the output of the classical bistable SR (CBSR) system is easily saturated. The piecewise nonlinear bistable SR (PNBSR) mode proposed by Gosak *et al.*[21] has achieved some results, but the potential barrier of this method has not completely broken the output saturation characteristic of CBSR. Lu *et al.*[22] proposed Woods–Saxon stochastic resonance (WSSR), which is a single potential well structure, the shape of the potential well can be adjusted by changing the system parameters. Jiao *et al.*[23] proposed an improved piecewise SR, the proposed method has a wider potential well and a lower wall steepness, which ensures that the particles have enough energy to continue to move upward during migration. Li *et al.*[24] used the combination of Woods and Gaussian potential well as the resonance model of SR. This model successfully detected the fault frequency of blade cracks. Zhang *et al.*[25] combined the Gaussian potential well model with a single potential well to form a new SR system. These improved models improve the detection ability of SR.

However, in the actual industrial measurement, there are often situations where the signal periodic force and the noise random force are very weak. At this time, using traditional models, it is often difficult to achieve particle transitions by adjusting system parameters to convert noise energy into signal energy. The SR model plays a key role in regulating the energy distribution of signals and noise in the system, therefore, it is of great practical significance to study a new SR model. To better improve the weak signal detection ability of SR, this paper proposes a new composite SR (NCSR) model combining the advantages of the improved piecewise bistable SR model and Woods–Saxon (WS) model. Although the improved piecewise model solves the problems of easy saturation and high intermediate potential barriers in classical traditional bistable models, the system stability will decrease as the model parameters change, and the problem of deepening the intermediate potential well in the model has also been exposed, which to some extent affects the ability of SR to enhance the signal. To address this issue, this article incorporates Woods into an improved piecewise model and constructs a novel composite SR model. The new model improves the extraction effect of weak characteristic signals by improving the dual effect of weak fault characteristics. The results show that the SR effect of the combination of improved piecewise model and WS model is better than that of using WS and traditional bistable

[†]Corresponding author. E-mail: jiaoshangbin@xaut.edu.cn

© 2024 Chinese Physical Society and IOP Publishing Ltd

SR methods and using only the improved piecewise model.

In the process of actual signal processing, the collected signals often have the characteristics of peak pulse and significant tail. According to the characteristics of such signals, scholars have studied the α stable distribution noise (also known as levy noise) model,[26–29] which not only contains the Gaussian distribution model,[30,31] but also can better match the actual data, and its application range is more extensive. So this paper mainly focuses on the research and application of the new composite SR model under α stable noise. This model has been applied to bearing fault diagnosis with good results. The NCSR model is introduced in Section 2, Section 3 is the simulation analysis of detection performance of NCSR system. In Section 4, experimental verification of NCSR system in image enhancement in made. Section 5 provides a summary of this paper.

2. New composite model

2.1. WS model

The WS is a nonlinear symmetric potential[32]

$$U_{\rm WS}(x) = -\frac{v}{1+\exp\left(\dfrac{|x|-r}{c}\right)}. \tag{1}$$

When $v=2$, $r=1$, and c has a variation range of 0.01–0.3, the WS potential well is shown in Fig. 1. From Fig. 1, it can be seen that when $c=0$, the potential is a square potential well, and as c increases, the wall of the potential well becomes smoother and smoother.

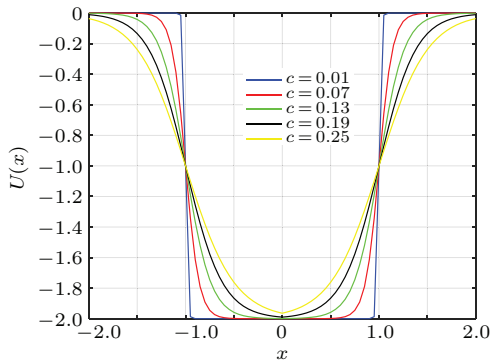


Fig. 1. The WS potential function.

2.2. Improved piecewise model

The piecewise model[23] is as follows:

$$U_1(x) = \begin{cases} \dfrac{-\sqrt{2}U_0}{m}(x+m) - U_0 - lx, & x < -m, \\ -\dfrac{a}{2}x^2 + \dfrac{b}{4}x^4 - lx, & -m \le x < 0, \\ -\dfrac{a}{2}x^2 + \dfrac{b}{4}x^4 + lx, & 0 \le x \le m, \\ \dfrac{\sqrt{2}U_0}{m}(x-m) - U_0 + lx, & x > m. \end{cases} \tag{2}$$

$U_1(x)$ is the potential function of the improved piecewise model, where a and b are the parameters of the model, $m = \sqrt{a/b}$, $U_0 = a^2/4b$, $l = k \times R_{\rm c}$, $0 \le k \le 1$. $R_{\rm c}$ is the input threshold of the system. Figure 2 shows a comparison between the two models.

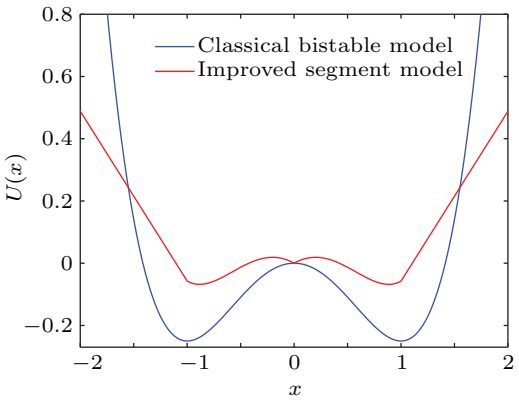


Fig. 2. A comparison diagram of the two models.

2.3. NCSR system

Combining the advantages of the above two models, an NCSR model is proposed, the new model overcomes the output saturation phenomenon of traditional bistability and is more conducive to particle leaps than the improved piecewise model.

$$U(x) = U_1(x) - U_{\rm ws}(x) = \begin{cases} \dfrac{-\sqrt{2}U_0}{m}(x+m) - U_0 - lx + \dfrac{V}{1+\exp\left(\dfrac{|x|-r}{c}\right)}, & x < -m, \\ -\dfrac{a}{2}x^2 + \dfrac{b}{4}x^4 - lx + \dfrac{V}{1+\exp\left(\dfrac{|x|-r}{c}\right)}, & -m \le x < 0, \\ -\dfrac{a}{2}x^2 + \dfrac{b}{4}x^4 + lx + \dfrac{V}{1+\exp\left(\dfrac{|x|-r}{c}\right)}, & 0 \le x \le m, \\ \dfrac{\sqrt{2}U_0}{m}(x-m) - U_0 + lx + \dfrac{V}{1+\exp\left(\dfrac{|x|-r}{c}\right)}, & x > m. \end{cases} \tag{3}$$

$U(x)$ is the potential function of the NCSR model. Figure 3(a) is a comparative diagram of Woods plus classical bistability and Woods plus improved piecewise model. Figure 3(b) is a three-dimensional graph of the NCSR model.

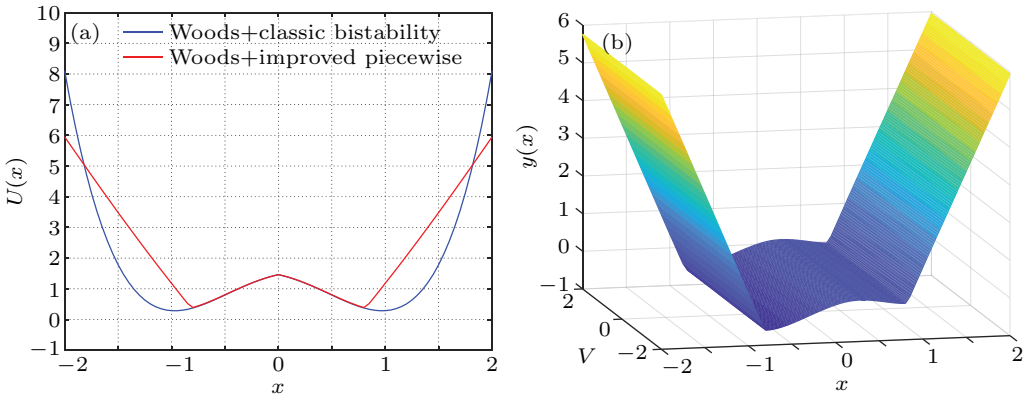


Fig. 3. Comparison diagram of two WS potential functions: NCSR model (a) and (b) NCSR model.

An NCSR system is studied in this paper. In the case of overdamping, the linear Langevin equation mainly relies on the damping term, while the inertia term can be ignored. If the damping coefficient is chosen as 1, then its dynamic equation is shown as follows:

$$\frac{\mathrm{d}x}{\mathrm{d}t} = -U'(x) + s(t) + D\eta_\alpha(t), \tag{4}$$

where $U(x)$ is the potential function of NCSR, $s(t)$ is a signal, $\eta_\alpha(t)$ represents the α stable noise, and D is the noise amplification factor which can change indirectly the intensity of $\eta_\alpha(t)$. Bring formula (3) into formula (4), we obtain

$$\frac{\mathrm{d}x}{\mathrm{d}t} = \begin{cases} \dfrac{\sqrt{2}U}{m} + l + \dfrac{V}{c}\mathrm{sgn}(x)\exp\left(\dfrac{|x|-r}{c}\right) \\ \times\left(1+\exp\left(\dfrac{|x|-r}{c}\right)\right)^{-2} + s(t) + D\eta_\alpha(t), \\ x < -m, \\ ax - bx^3 + l + \dfrac{V}{c}\mathrm{sgn}(x)\exp\left(\dfrac{|x|-r}{c}\right) \\ \times\left(1+\exp\left(\dfrac{|x|-r}{c}\right)\right)^{-2} + s(t) + D\eta_\alpha(t), \\ -m \le x < 0, \\ ax - bx^3 - l + \dfrac{V}{c}\mathrm{sgn}(x)\exp\left(\dfrac{|x|-r}{c}\right) \\ \times\left(1+\exp\left(\dfrac{|x|-r}{c}\right)\right)^{-2} + s(t) + D\eta_\alpha(t), \\ 0 \le x \le m, \\ -\dfrac{\sqrt{2}U}{m} - l + \dfrac{V}{c}\mathrm{sgn}(x)\exp\left(\dfrac{|x|-r}{c}\right) \\ \times\left(1+\exp\left(\dfrac{|x|-r}{c}\right)\right)^{-2} + s(t) + D\eta_\alpha(t), \\ x > m. \end{cases} \tag{5}$$

Solving Eq. (5) with the fourth-order Runge–Kutta algorithm, the value of x is the output of the NCSR system.[33]

2.4. Detection scheme of NCSR system

In signal detection, the signal, noise, nonlinear system can achieve the best matching effect by adjusting the parameters of the NCSR system. To further achieve the best results, the NCSR system adopts differential brain storming optimization (DBSO)[34] algorithm to optimize the six parameters of a, b, l, v, r, c, and takes the output SNR (characteristic coefficient) as the fitness function. The flow chart of DBSO is shown in Fig. 4 and the detection scheme based on the NCSR system is shown in Fig. 5.

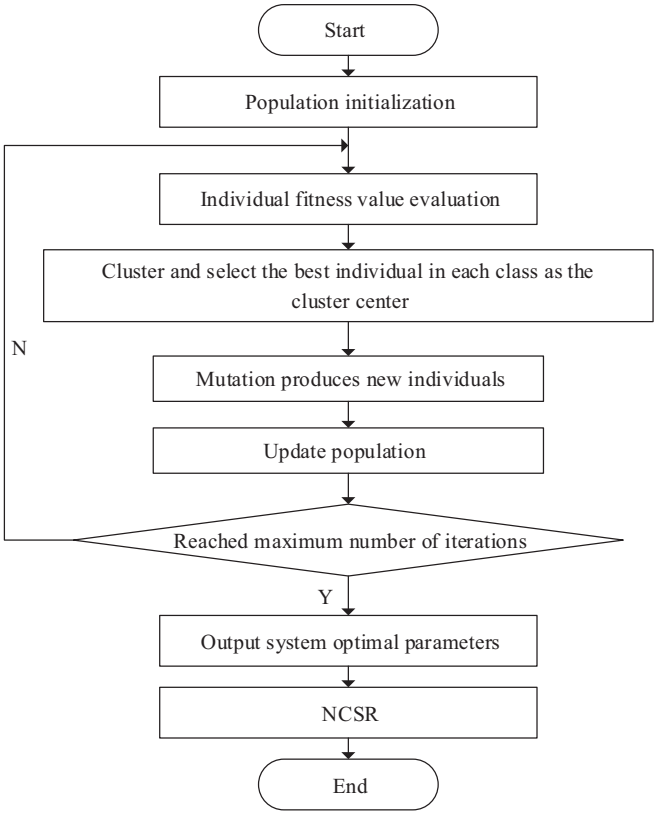


Fig. 4. Flow chart of NCSR based on DBSO.

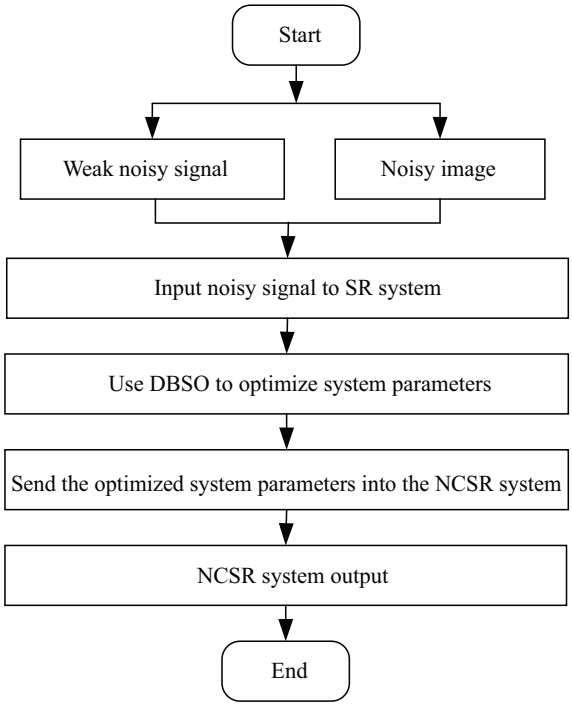


Fig. 5. Detection scheme based on NCSR system.

3. Simulation analysis and evaluation of NCSR system

3.1. System performance analysis

3.1.1. NCSR in α stable noise environment

In α stable noise environment, the influence of NCSR system parameters a, b, l, v, r, c on the output SNR under the action of different characteristic exponents α ($0 < \alpha \leq 2$) and symmetric parameters β ($-1 \leq \beta \leq 1$) is analyzed. The following system simulation settings $f_s = 4.08$ Hz, $N = 4096$, and noise intensity $D = 0.3$.

(I) Influence of characteristic index α on SR effect

The α steady noise fixed distribution parameters $\beta = 0$, $\sigma = 1$, $\mu = 0$, the characteristic index is taken as 0.8, 1, 1.5 respectively. When $b = 1$, $l = 0.5$, $v = 2.5$, $r = 1$, $c = 5$, the curve of a changing with SNR is shown in Fig. 6(a). When $a = 10$, $l = 0.5$, $v = 2.5$, $r = 1$, $c = 5$, the curve of b changing with SNR is shown in Fig. 6(b). The drawing methods of Figs. 6(c)–6(e) are the same as those of Figs. 6(a) and 6(b), and the values of the fixed parameters are consistent with those of Figs. 6(a) and 6(b).

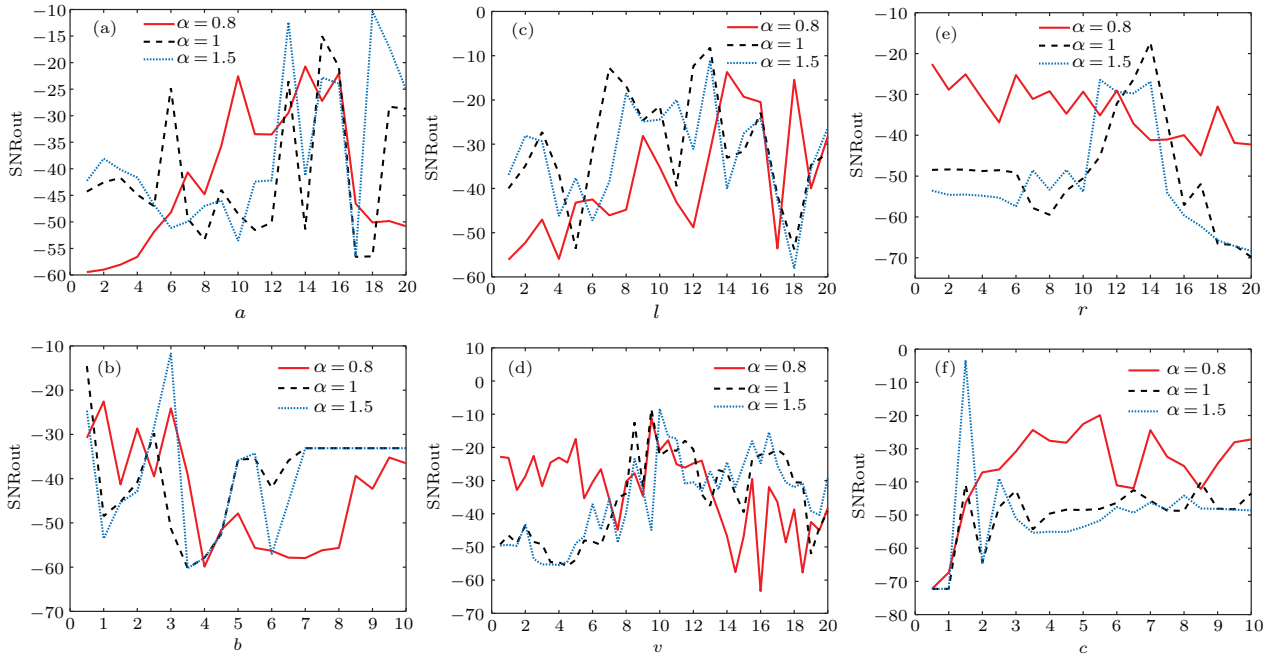


Fig. 6. Variation curves of parameters under different α actions.

In Fig. 6, the SNR shows a typical curve of SR characteristics with the change of different parameters, which indicates that different system parameters can induce SR in α stable noise environment, and promote the transmission of noise energy to useful signals, so that weak signals to be measured can be enhanced and detected. At the same time, it can be found that when in the optimal resonance range, the larger the characteristic index α of stable noise, the greater the output SNR value of the system. This is because the smaller the characteristic index α, the more significant the impact characteristics of α stable noise, and the greater the degree of submergence of useful signals.

(ii) Influence of symmetry parameter β on SR effect

The fixed distribution parameters of the α stable noise, $\alpha = 1.2$, $\sigma = 1$, $\mu = 0$, and symmetrical parameters β are taken as -1, 0, and 1 respectively. The values and methods of other parameters are consistent with the above, under the action of different symmetrical parameters β, figures 7(a)–7(e) are the same as Figs. 6(a)–6(e) for the drawing method and the fixed parameters.

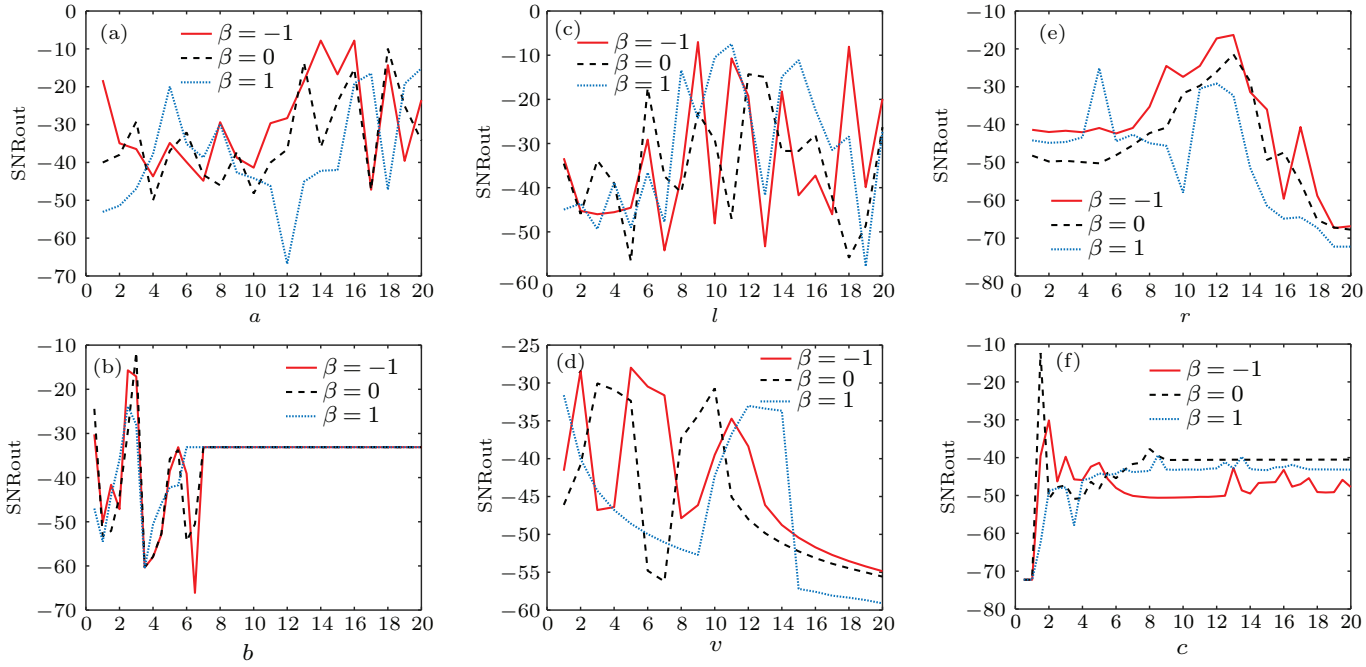


Fig. 7. Variation curves of parameters under different β actions.

From Figs. 7, it can be seen that the variation of symmetric parameter β does not affect the optimal system parameter range, and the SNR value at $\beta=0$ is greater than that at $\beta\neq 0$, indicating that the SR effect is better when the stable noise is symmetrically distributed than that when it is asymmetric. In Fig. 7(d), multiple peaks in the output SNR appear, indicating the occurrence of multiple random resonance phenomena.

3.1.2. Performance analysis of NCSR systems

Take the signal $s(t)=A\sin(2\pi ft)$, $A=0.1$, $=0.01$ Hz, α noise interval is [0,2]. Figure 8 shows the average of 20 experiments, the parameters of improved piecewise model system are $a=10$, $b=1$, $l=0.5$, and the parameters of NCSR system are $a=10$, $b=1$, $l=0.5$, $v=2.5$, $r=1$, $c=5$. As can be seen from Fig. 8 that the output SNR of the NCSR model is higher than that of the improved piecewise model with the same parameter values in α noise environments. Therefore, NCSR system can improve the detection effect of weak signal, match the best SR model more easily, and have better processing capabilities compared with the improved piecewise system.

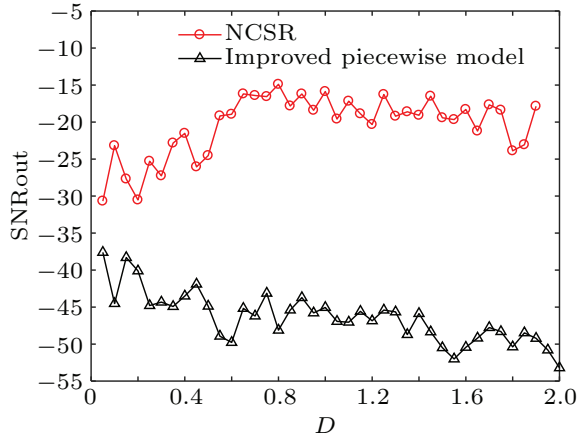


Fig. 8. The variation curve of SNR with D under α stable noise.

3.2. Simulation and analysis of periodic signals in NCSR system

The α stable noise has the characteristics of spikes and is therefore closer to the actual noise. The impact of the NCSR system on the periodic signal output is analyzed in α stable noise environment with the SNR as the measurement index. Set $f_s=4.08$ Hz and $N=4096$ in the system simulation below, and DBSO is used for system parameter optimization.

3.2.1. Single low-frequency

The simulation signal $s(t)=A\sin(2\pi ft)+n(t)$, $A=0.1$, $f=0.01$ Hz, and $D=0.3$. Figures 9(a) and 9(b) are time domain and power spectrum diagrams of noisy signals with input SNR of -30.2771 dB. Using the detection scheme shown in Fig. 5, the optimization parameters are $a=0.6302$, $b=0.2051$, $l=0.1513$, $v=-0.2301$, $r=1.528$, $c=2.9965$. Figures 9(c) and 9(d) are time domain and power spectrum of the output signal, NCSR system output SNR is -4.882 dB, an increase of 25.3951 dB.

3.2.2. Multiple low frequency

For multiple signals $s(t)=A_1\sin(2\pi f_1t)+A_2\sin(2\pi f_2t)+A_3\sin(2\pi f_3t)+n(t)$, $A=0.3$, $f_1=0.01$ Hz, $f_2=0.02$ Hz, $f_3=0.05$ Hz, $D=0.3$. The time domain and power spectrum diagrams of the input noisy signal are shown

in Figs. 10(a) and 10(b), and the input SNR is −29.3874 dB. The optimization parameters are $a = -2.036$, $b = 7.835$, $l = 10$, $v = -5.704$, $r = 21.1157$, $c = 14.1832$. The time-domain and power spectrum of the output signal through the NCSR system are shown in Figs. 10(c) and 10(d), NCSR system output SNR is −8.6374 dB, an increase of 20.75 dB.

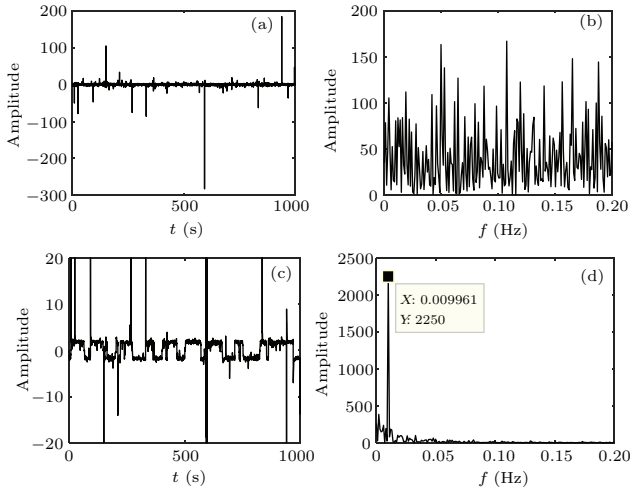


Fig. 9. Analysis results of simulation signals in α noise: (a) input signal waveform, (b) input signal spectrum, (c) output signal waveform, (d) output signal spectrum.

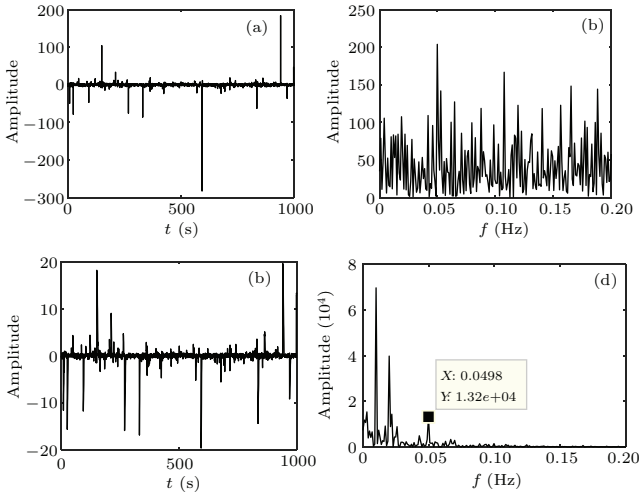


Fig. 10. Analysis results of simulation signals in α noise: (a) input signal waveform, (b) input signal spectrum, (c) output signal waveform, (d) output signal spectrum.

3.2.3. Single high-frequency

When researching the NCSR driven by single high-frequency signals, $s(t) = A\sin(2\pi ft) + n(t)$, $A = 0.1$, $f = 100$ Hz, $D = 0.3$, and $f_s = 40.8$ kHz. Figures 11(a) and 11(b) are time domain and power spectrum diagrams of noisy signals with input SNR of −30.2771 dB. Send noisy signals into the NCSR system using the detection process shown in Fig. 5. Optimized system parameters are $a = 0.7034$, $b = -7.1447$, $l = 7.6467$, $v = -7.239$, $r = 9.3633$, $c = 13.0307$, the time domain and power spectrum of the output signal through the NCSR system are shown in Figs. 11(c) and 11(d), NCSR system output SNR is −6.0914 dB, an increase of 24.1857 dB.

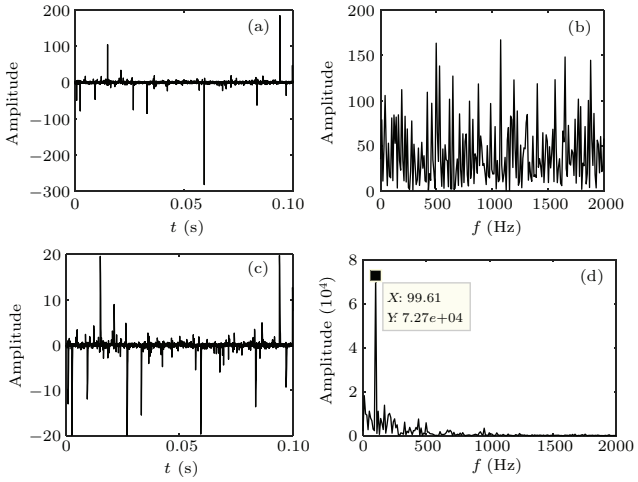


Fig. 11. Analysis results of simulation signals in α noise: (a) input signal waveform, (b) input signal spectrum, (c) output signal waveform, (d) output signal spectrum.

3.2.4. Multiple high-frequency

For multiple high-frequency periodic signals, $A_1 = A_2 = A_3 = 0.1$, $f_1 = 100$ Hz, $f_2 = 200$ Hz, $f_3 = 500$ Hz, $s(t) = A_1\sin(2\pi f_1 t) + A_2\sin(2\pi f_2 t) + A_3\sin(2\pi f_3 t) + n(t)$, $D = 0.3$, $f_s = 40.8$ kHz, figures 12(a) and 12(b) are time domain and power spectrum of noisy signal with input SNR of −29.3874 dB. It is passed through the NCSR system as shown in Figs. 12(c) and 12(d). The optimization parameters are $a = 4.1942$, $b = -16.2739$, $l = -14.3402$, $v = -5.9602$, $r = 12.3326$, $c = 30.5754$, system output SNR is −9.85 dB, an increase of 19.5374 dB.

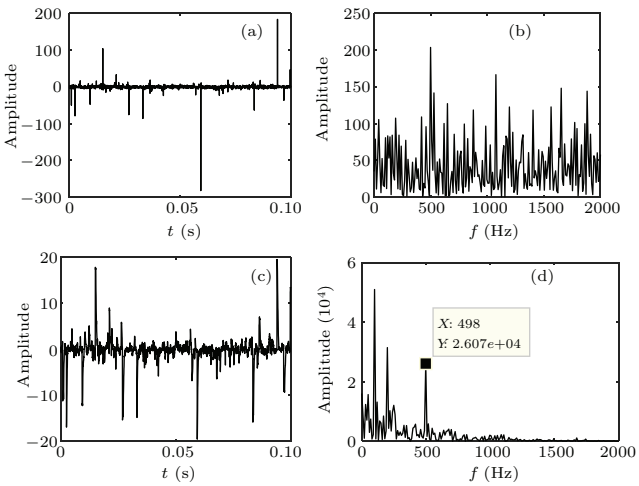


Fig. 12. Analysis results of simulation signals in α noise: (a) input signal waveform, (b) input signal spectrum, (c) output signal waveform, (d) output signal spectrum.

Figures 9–12(a) are the time domain diagrams of mixed signal of the signal to be measured, α stable noise and the external signal, and figures 9–12(b) are the corresponding power spectrum diagrams, from which no useful information of the

signal can be obtained. Figures 9–12(c) are the time domain diagrams of the NCSR system output signal, figures 9–12(d) are the power spectrum of the system output signal, the frequency close to the signal to be measured can be clearly observed, the amplitude of the signal to be measured is amplified, which indicates that the NCSR system has achieved a good match and detection of periodic signals under α noise.

3.3. Simulation and analysis of aperiodic signals in NCSR system

The previous section verified that NCSR has a good detection effect on weak periodic signals, but in practice, many signals are aperiodic signals, such as impact signals, ultrasonic signals, and ultra wide band, and so on. Therefore, it is of great significance to use NCSR to achieve effective detection of aperiodic signals. This section studies the adaptive SR driven by aperiodic signal under α noise environment, the adaptive detection of aperiodic impact signal and ultrasonic signal are realized respectively, and the optimal potential well shape of NCSR is analysed.

3.3.1. Impact signal detection

To observe the response of the NCSR model induced by the periodic impact signal under α noise, the expression of aperiodic impact signal[35] is

$$s(t) = A\exp\left(-3\left(\frac{t-t_0}{\tau}\right)^2\right). \tag{6}$$

The given impact signal parameters are $A = 1.5$, $\tau = 1$, $t_0 = 10$, by adding α noise with intensity of $D = 0.1$, the adaptive NCSR system is used to process noisy impact signals, the optimized system parameters are $a = 9.0507$, $b = 2.4975$, $l = 0.0001$, $v = -0.2339$, $r = 2.2759$, $c = 0.8957$.

As shown in Fig. 13(b) that the pure impact signal is submerged by noise, and the location of the shock signal cannot be seen in the noisy signal. However, through the adaptive NCSR system, an impact signal with a peak height of 1.936 appears at $t_0 = 10.25$, in Fig. 13(c), NCSR can effectively detect noisy impact signal.

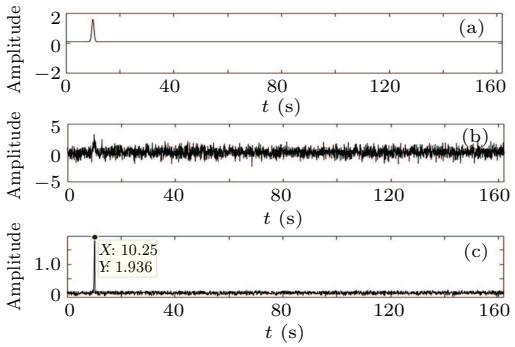


Fig. 13. Detection results of impact signal: (a) impact signal, (b) noisy impact signal, (c) NCSR system output.

3.3.2. Ultrasonic signal detection

The expression of the ultrasonic signal[36] is as follows:

$$s(t) = \frac{A}{2}\left[1-\cos\left(\frac{2\pi ft}{n}\right)\right]\sin(2\pi ft). \tag{7}$$

The given ultrasonic signal parameters $A = 0.012$, $f = 0.05$ Hz, $n = 10$, $D = 0.04$, the noisy ultrasound signal is shown in Figs. 14(a) and 14(b), the input SNR is -28.6209 dB. It shows that the ultrasonic signal has been submerged by noise, and its signal characteristics are not observed. Input the noisy signal into the NCSR system, set $f_s = 25$ Hz, $N = 5000$, the optimization parameters of the system are $a = 5$, $b = 2.6415$, $l = 0.0001$, $v = -8.925$, $r = 0.7079$, $c = 2.5491$, the NCSR system output is shown in Figs. 14(c) and 14(d) and its output SNR is -5.7705 dB, an increase of 22.8504 dB. The impact component of the ultrasonic signal can be observed in Fig. 14(c), but the curve has a certain degree of distortion. In the power spectrum of Fig. 14(d), a high spectral peak value appears at $f = 0.05$ Hz, which is consistent with the frequency of the input signal, indicating that the NCSR system can achieve the detection of ultrasonic signal.

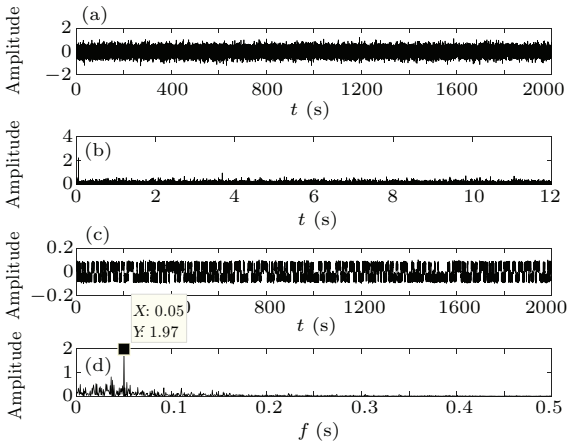


Fig. 14. Detection results of ultrasonic signal: (a) input signal waveform, (b) input signal spectrum, (c) output signal waveform, (d) output signal spectrum.

4. Application in image enhancement

In order to verify the application of the new model in practical engineering, the new model is applied to image denoising, the basic principle of image processing based on NCSR is shown in Fig. 15. Taking noise images from three common noise environments as examples, the traditional linear filtering method and nonlinear filtering method are used for denoising comparison respectively. Figure 15 shows the denoising results of the noisy images by the mean filtering, median filtering, wiener filtering, improved piecewise SR, and NCSR method.

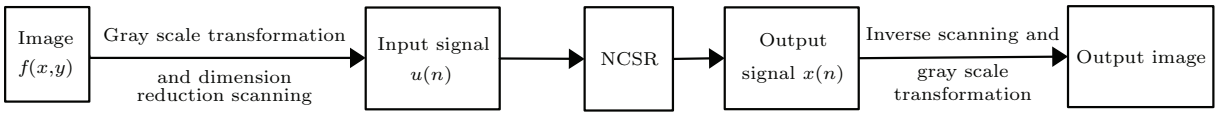


Fig. 15. Basic principle of NCSR image processing.

In simulation experiments, peak signal-to-noise ratio (PSNR) is used to evaluate image quality. The larger the value of PSNR, the smaller the difference from the original reference image, and the higher the quality of the image. The correlation number (C) is the degree of similarity between the output image of the system and the original image. The larger C, the higher the restoration degree of the processed image, and the maximum C is 1. The expressions for PSNR and C are

$$\mathrm{PSNR} = 10 \times \log_{10}\left(\frac{(2^n-1)^2}{\mathrm{MSE}}\right), \tag{8}$$

$$C(X,Y) = \frac{\mathrm{Cov}(X,Y)}{\sqrt{D(X)D(Y)}}. \tag{9}$$

4.1. Gaussian noise

Figure 16(a) is a Lena diagram with Gaussian noise with noise intensity of 0.1, the PSNR of the noise image is 11.105 dB. Figures 16(b), 16(c), and 16(d) are the results of image denoising under three common linear noises, figure 16(e) is the image denoising result of nonlinear improved piecewise SR, figure 16(f) is the result of image denoising using NCSR. Through the comparison of the above methods, it can be seen that NCSR has better denoising effect on the image. The optimization parameters of NCSR are $(a,b,l,v,r,c) = (1.4621, 3.9104, 10, -7.2049, -7.7496, 17.7525)$. The similarity between the denoised image and the original image (correlation number) is 0.976, and the PSNR of the image is improved by 10.285 dB compared with the noisy image.

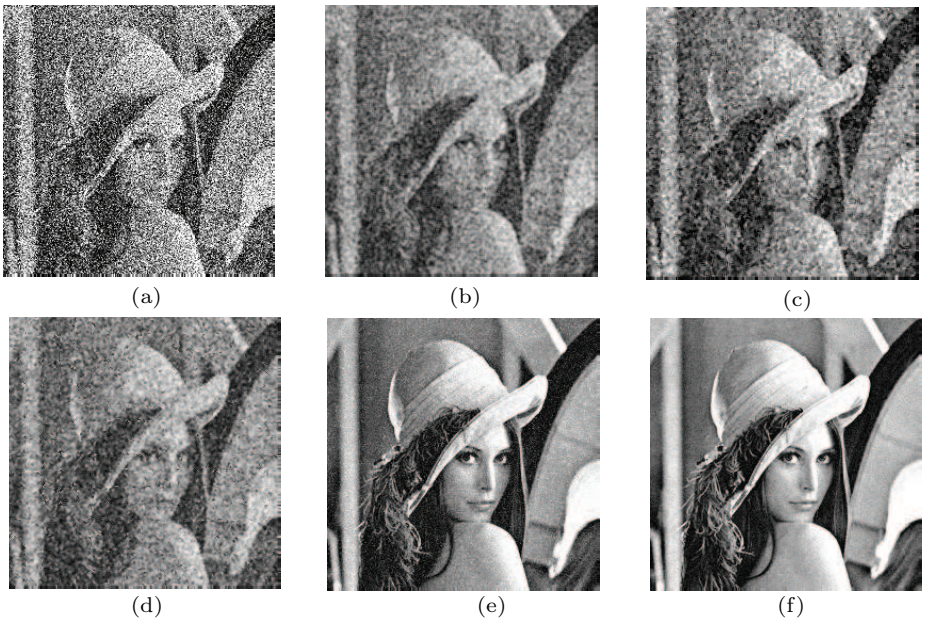


Fig. 16. Image processing results of different denoising methods: (a) noisy image, (b) mean filtering, (c) median filtering, (d) wiener filtering, (e) improved piecewise SR, (f) NCSR.

Table 1. Comparison of different denoising methods for noisy images.

	Noisy image	Mean filtering	Median filtering	Wiener filtering	Improved piecewise SR	NCSR
Correlation number C		0.8405	0.7904	0.8011	0.9416	0.976
PSNR (dB)	11.1050	18.5278	18.9984	17.3206	19.8598	21.3900

4.2. Salt and pepper noise

Figure 17(a) is a Lena diagram with salt and pepper noise with noise intensity of 0.2, the PSNR of the noise image is 12.0888 dB. Figures 17(b)–17(d) are the results of image denoising under three common linear noises, figure 17(e) is the image denoising result of nonlinear improved piecewise SR, and figure 17(f) is the result of image denoising using NCSR. Through the comparison of the above methods, it can be seen that NCSR has better denoising effect on the image. The optimization parameters of NCSR are $(a,b,l,v,r,c) = (0.8354, 8.0847, 1.9894, -3.0793, -9.2941, 3.9367)$. The correlation number is 0.9505, and the PSNR of the image is improved by 7.6204 dB compared with the noisy image.

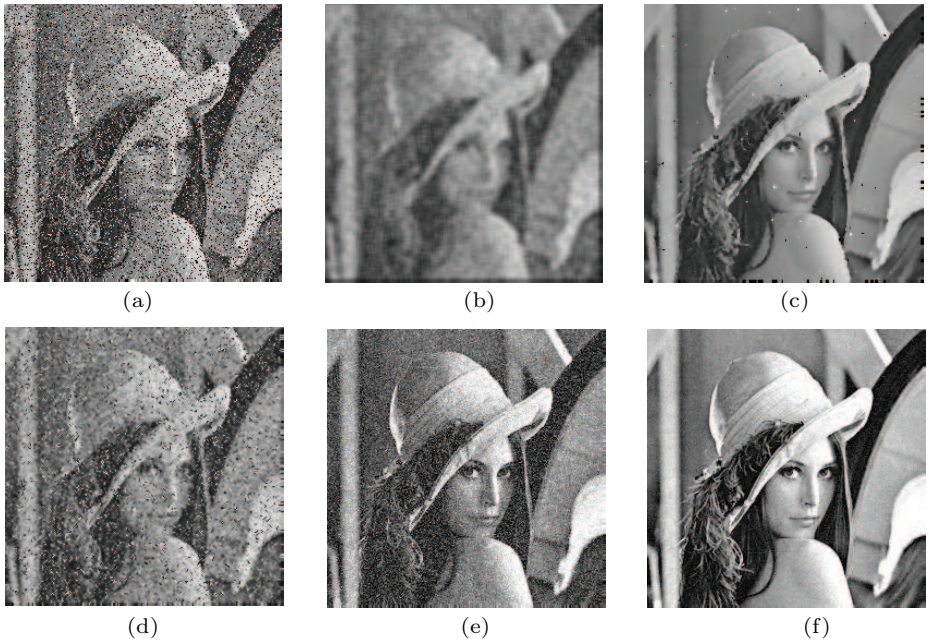


Fig. 17. Image processing results of different denoising methods: (a) noisy image, (b) mean filtering, (c) median filtering, (d) wiener filtering, (e) improved piecewise SR, (f) NCSR.

Table 2. Comparison of different denoising methods for noisy images.

	Noisy image	Mean filtering	Median filtering	Wiener filtering	Improved piecewise SR	NCSR
Correlation number C		0.8895	0.9077	0.7619	0.9238	0.9505
PSNR (dB)	12.0888	18.6294	18.9466	16.3473	19.6154	19.7092

4.3. Multiplicative noise (speckle noise)

Figure 18(a) is a Lena diagram with multiplicative noise (speckle noise) with noise intensity of 0.1, the PSNR of the noise image is 13.0255 dB. Figures 18(b), 18(c), and 18(d) are the results of image denoising under three common linear noises, figure 18(e) is the image denoising result of nonlinear improved piecewise SR, figure 18(f) is the result of image denoising using NCSR. Through the comparison of the above methods, it can be seen that NCSR has better denoising effect on the image. The optimization parameters of NCSR are $(a,b,l,v,r,c) = (2.779, 3.0548, 14.4208, -7.9809, 3.69760.6625, 2.9355)$. The correlation number is 0.9956, and the PSNR of the image is improved by 7.1121 dB compared with the noisy image.

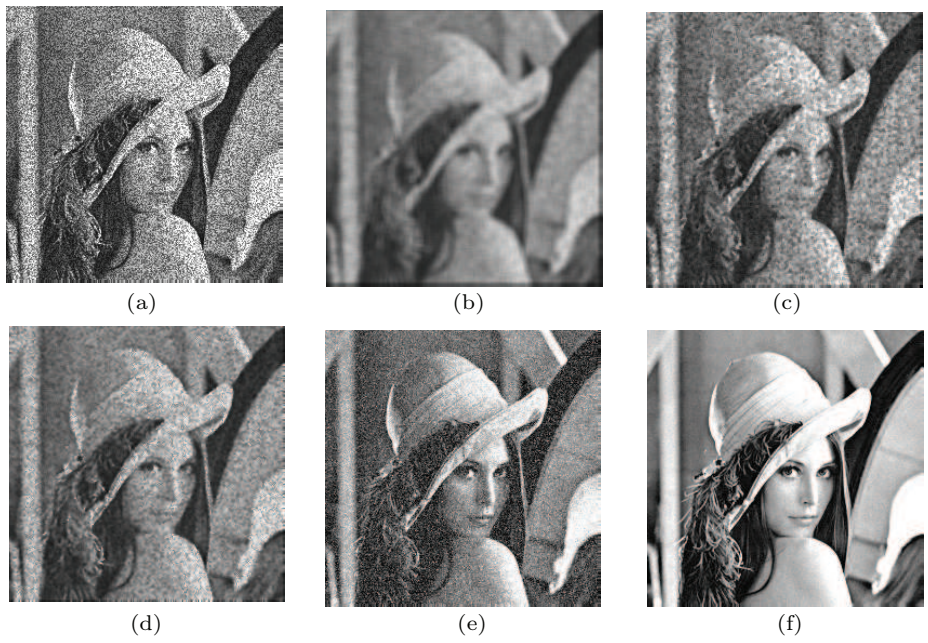


Fig. 18. Image processing results of different denoising methods: (a) noisy image, (b) mean filtering, (c) median filtering, (d) wiener filtering, (e) improved piecewise SR, (f) NCSR.

Table 3. Comparison of different denoising methods for noisy images.

	Noisy image	Mean filtering	Median filtering	Wiener filtering	Improved piecewise SR	NCSR
Correlation number C		0.9049	0.8740	0.8480	0.9235	0.9956
PSNR (dB)	13.0255	19.4246	19.6449	18.8237	19.7682	20.1376

5. Conclusion

In order to improve the detection performance of weak signal of SR in strong noise background, a new composite SR model is proposed in this paper. The main work of this paper is as follows: (i) Combining the advantages of Woods–Saxon model and improved piecewise model, a new composite SR model (NCSR) is proposed. (ii) Under α stable noise environment, the new model is used to detect periodic signals. The detection results show that the model is applicable to the detection of periodic signals. (iii) Under α stable noise environment, the impulse signal and ultrasonic wave in the aperiodic signal are detected, the detection results show that the model is also applicable to the detection of aperiodic signals. (iv) The new model SR system is applied to image denoising, and compared with traditional denoising methods and improved piecewise SR denoising methods, the model has better denoising effect, higher output PSNR, and similarity. This model further enriches the theory of SR, and applies the new model to the image denoising process, which promotes the application of SR in practice.

Acknowledgements

Project supported by the National Natural Science Foundation of China (Grant No. 62371388) and the Key Research and Development Projects in Shaanxi Province, China (Grant No. 2023-YBGY-044).

References

[1] Benzi R, Sutera A and Vulpiani A 1981 *J. Phys. A: Math. Gen.* **14** L453
[2] Mantegna R and Spagnolo B 1995 *Nuovo Cimento D* **17** 873
[3] Wiesenfelda K and Jaramillob F 1998 *Chaos* **8** 539
[4] Harmer G P, Davis B R and Abbott D 2002 *IEEE Trans. Instrum Meas* **51** 299
[5] Dong H T, Shen X H, Hea K and Wang H Y 2020 *Chaos, Solitons and Fractals* **141** 110428
[6] Xu B H, Duan F B, Bao R H and Li J L 2002 *Chaos, Solitons Fractals* **13** 633
[7] Zhou Z B, Yu W X and Wang J N 2022 *Chaos, Solitons and Fractals* **154** 111642
[8] Yao Y G 2021 *Chin. Phys. B* **30** 060503
[9] Qiao Z J, Elhattab A, Shu X D and He C B 2021 *Nonlinear Dyn.* **106** 707
[10] Qiao Z J, He Y B, Liao C R and Zhu R H 2023 *Chaos, Solitons and Fractals* **175** 113960
[11] Qiao Z J, Lei Y G and Li N P 2019 *Mech. Syst. Signal Process.* **122** 502
[12] Lu S L, He Q B and Wang J 2019 *Mech. Syst. Signal Process.* **116** 230
[13] Semenova N, Porte X, Andreoli L, Jacquot M, Larger L and Brunner D 2019 *Chaos* **29** 103128
[14] Duan L L, Duan F B, Chapeau-Blondeau F and Abbott D 2020 *Phys. Lett. A* **384** 126143
[15] Chen Z J, Duan F B, Chapeau-Blondeau F and Abbott D 2022 *Phys. Lett. A* **432** 128008
[16] Semenova N and Brunner D 2022 *Chaos* **32** 061106
[17] Audhkhasi K, Osoba O and Kosko B 2016 *Neural Netw.* **78** 15
[18] Valenti D, Schimansky-Geier L, Sailer X and Spagnolo B 2006 *Eur. Phys. J. B* **50** 199
[19] Wiesenfeld K and Moss F 1995 *Nature* **373** 33
[20] Qiao Z J, Lei Y G, Lin J and Jia F 2017 *Mech. Syst. Signal Process.* **84** 731
[21] Goask M, Perc M and Kralj S 2011 *Eur. Phys. J. B* **80** 519
[22] Lu S L, He Q B and Kong F R 2014 *Mech. Syst. Signal Process.* **45** 488
[23] Jiao S B, Lei S, Jiang W, Zhang Q and Huang W C 2019 *IEEE Access* **7** 160191
[24] Li H K, He C B, Malekian R and Li Z X 2018 *Sensors* **18** 1264
[25] Zhou Y H, Xu X M, Yin L Z, Ding Y P, Ding J F and Sun K H 2020 *Chin. Phys. B* **29** 040503
[26] La Cognata A, Valenti D, Dubkov A A and Spagnolo B 2010 *Phys. Rev. E* **821** 011121
[27] Guarcello C 2021 *Chaos, Solitons and Fractals* **153** 111531
[28] Lisowski B, Valenti D, Spagnolo B, Bier M and Gudowska-Nowak E 2015 *Phys. Rev. E* **91** 042713
[29] Li QQ, Xu X M, Lin Z Y, Ding Y P, Ding J F and Sun K H 2018 *Chin. Phys. B* **27** 034203
[30] Guarcello C, Valenti D, Spagnolo B, Pierro V and Filatrella G 2019 *Phys. Rev. Appl.* **11** 044078
[31] Guo Y F, Wang L J, Wei F and Tan J G 2020 *Indian J. Phys.* **94** 1625
[32] Mi L N, Guo Y F, Zhang M and Zhuo X J 2023 *Chaos, Solitons and Fractals* **167** 113096
[33] Zhou Y H, Xu X M, Yin L Z, Ding Y P, Ding J F and Sun K H 2020 *Chin. Phys. B* **29** 040503
[34] Mateos J L and Alatriste F R 2021 *Chaos* **21** 047503
[35] Jiao S B, Qiao X X, Lei S and Jiang W 2019 *Chin. J. Phys.* **59** 138
[36] Siqueira M H S, Gatts C E N, Silva R R D and Rebello J M A 2004 *Ultrasonics* **41** 785